Proc. Natl. Acad. Sci. USA
Vol. 95, pp. 7789–7794, June 1998
Physiology

Conformational changes couple Na^+ and glucose transport

(glucose cotransporter/glucose–galactose malabsorption/fluorescence microscopy/methanethiosulfonate reagents)

DONALD D. F. LOO*†, BRUCE A. HIRAYAMA*, ELSA M. GALLARDO, JASON T. LAM, ERIC TURK, AND ERNEST M. WRIGHT

Department of Physiology, University of California Los Angeles School of Medicine, Center for the Health Sciences, Los Angeles, CA 90095-1751

Edited by Joseph F. Hoffman, Yale University School of Medicine, New Haven, CT, and approved April 20, 1998 (received for review March 11, 1998)

ABSTRACT **The mechanism by which cotransport proteins couple their substrates across cell membranes is not known. A commonly proposed model is that cotransport results from ligand-induced conformational transitions that change the accessibility of ligand-binding sites from one side of the membrane to the other. To test this model, we have measured the accessibility of covalent probes to a cysteine residue (Q457C) placed in the putative sugar-translocation domain of the Na^+/glucose cotransporter (SGLT1). The mutant protein Q457C was able to transport sugar, but transport was abolished after alkylation by methanethiosulfonate reagents. Alkylation blocked sugar translocation but not sugar binding. Accessibility of Q457C to alkylating reagents required external Na^+ and was blocked by external sugar and phlorizin. The voltage dependence of accessibility was directly correlated with the presteady–state charge movement of SGLT1. Voltage-jump experiments with rhodamine-6-maleimide-labeled Q457C showed that the time course and level of changes in fluorescence closely followed the presteady–state charge movement. We conclude that conformational changes are responsible for the coupling of Na^+ and sugar transport and that Q457 plays a critical role in sugar translocation by SGLT1.**

Cotransporters are a major class of membrane proteins that are formed by members of several gene families. They share the common property of being able to couple the electrochemical potential gradient of a cation (Na^+ or H^+) to transport of organic solutes, ions, and water uphill into cells (see refs. 1 and 2). Although the mechanism of energy transduction is unknown, cotransporters share several common functional properties. For example, they exhibit presteady–state currents with step changes in membrane potential, which suggests the existence of a common mechanism.

Kinetic models of cotransport have been proposed. Most popular are: alternating access models in which binding of multiple substrates at distinct sites that are only accessible on one side of the membrane at a time; transport then occurs via ligand and voltage induced conformational changes (3, 4); and channel-like models with multiple substrate occupancy without conformational changes (5). Mathematical simulations of each type of model can account for many experimental observations. In the alternating access model, the presteady–state currents are caused by both relaxations of charged or polar residues in the protein in response to voltage perturbations and movement of the transported ions in the membrane field (4, 6). In contrast, in the channel model, presteady–state currents are strictly caused by the transported ions (5).

The advent of cysteine mutagenesis and derivatization with probe reagents has proved to be a useful tool for structure/function studies of ion channels and transporters (7–9), and membrane voltage has been found to affect the accessibility of residues in the transmembrane domain (8, 10). The dependence of cotransport function on both substrates and membrane voltage suggested to us that a properly placed probe would allow us to test the alternating access model for the Na^+/glucose cotransporter (SGLT1). Our strategy was to measure the accessibility of covalent probes to a cysteine residue placed in the putative sugar-translocation domain of SGLT1. The alternating access model predicts that accessibility to critical residues would depend on the conformational state of the protein and that accessibility should be influenced by ligands and membrane voltage.

Glutamine 457 is a critical residue because the mutation Q457R causes glucose–galactose-malabsorption (GGM) by blocking sugar translocation (ref. 11 and M. P. Lostao, unpublished results). We have found that the new construct Q457C retains full Na^+/glucose cotransport activity and that chemical mutagenesis (alkylation) of Q457C fully recapitulates the GGM phenotype. Q457C is in transmembrane helix 11 (TMH 11) at the interface between the membrane and the extracellular fluid (12, 13), and TMH 11 is one of four C-terminal helices (TMH 10–13) thought to form the sugar translocation domain (14). We found that accessibility of Q457C to alkylating reagents depended on ligands (Na^+, sugar, and phlorizin). Voltage-jump experiments with rhodamine-6-maleimide-labeled Q457C showed that the presteady–state charge movements of the protein closely followed the changes in fluorescence. The presteady–state charge movement also was correlated directly with changes in accessibility. We conclude that conformational changes are responsible for the coupling of Na^+ and sugar transport.

MATERIALS AND METHODS

Molecular Biology. Wild-type human SGLT1 cDNA was mutagenized by PCR (11) with the oligonucleotide primers Q457C-sense: 5′-CTT CGA TTA CAT C**TG C**TC CAT CAC CAG T 3′ and Q457C-antisense: 5′-ACT GGT GAT CGA **GCA** GAT GTA ATC GAA G 3′. The bold letters represent the mutation at amino acid position 457 to a cysteine. Two

The publication costs of this article were defrayed in part by page charge payment. This article must therefore be hereby marked "*advertisement*" in accordance with 18 U.S.C. §1734 solely to indicate this fact.

This paper was submitted directly (Track II) to the *Proceedings* office.

Abbreviations: GGM, glucose–galactose-malabsorption; TMH, transmembrane helix; SGLT1, Na^+/glucose cotransporter; αMDG, α-methyl-D-glucopyranoside; MTS, methanethiosulfonate; MTSEA, 2-aminoethyl methanethiosulfonate hydrobromide; MTSES, sodium(2-sulfonatoethyl)methanethiosulfonate; MTSET, 2-(trimethylammonium)ethyl methanethiosulfonate bromide; MMTS, methyl methanethiosulfonate; TMR6M, tetramethylrhodamine-6-rhodaminemaleimide; TMR5M, tetramethylrhodamine-5-maleimide; NEM, *N*-ethylmaleimide.

*D.D.F.L. and B.A.H. contributed equally to this work.
†To whom reprint requests should be addressed. e-mail: dloo@physiology.medsch.ucla.edu.

mutagenized PCR products were obtained in two separate reactions by using either mutagenizing primer with a downstream nonmutagenic primer. These two PCR products were gel purified and then combined in a final PCR reaction by using the same normal primers flanking the mutation site to produce an insert with flanking *Xcm*I restriction sites. This final fragment was then cut with *Xcm*I, gel purified, and ligated to an *Xcm*I-digested, alkaline phosphatase-treated wild-type construct. A transformed colony was screened by sequencing through the *Xcm*I sites to verify the presence of only the desired mutation.

Mature *Xenopus laevis* oocytes were injected with 25–50 ng of capped cRNA (MessageMachine or MegaScript, Ambion, Austin, TX) coding for human SGLT1 or the cysteine mutation Q457C (6). Oocytes were incubated in Barth's medium containing 1 mg/ml gentamicin, 10 μM EDTA, and 500 μM DTT at 18°C for 3–14 days.

Labeling by Methanethiosulfonate (MTS) and Maleimide Derivatives. MTS and maleimide reagent stocks were prepared each day at 5–20 mM in anhydrous methanol or dimethyl sulfoxide and diluted to the desired concentration immediately before use. Concentrations of MTS reagents or NEM (*N*-ethylmaleimide) > 1 mM were dissolved in buffer immediately before use. Concentrations of methanol or dimethyl sulfoxide did not exceed 1%. Control experiments with methanol or dimethyl sulfoxide at 1% concentration had no effect on transporter function. The transport level at saturating αMDG (α-methyl D-glucopyranoside, 10 mM for wild-type SGLT1, and 50–200 mM for Q457C) was measured before labeling. Labeling was performed with the oocyte membrane clamped to a specified voltage, and then the reagent was added to the bath solution. At the end of the labeling period, the reagents were rapidly flushed from the chamber and membrane potential was returned to the normal holding value V_h (−50 mV). Extent of derivatization of C457 was determined by the reduction in sugar-dependent current at −50 mV and saturating sugar concentrations for the transporter. The MTS reagents MTSEA (2-aminoethyl methanethiosulfonate hydrobromide), MTSES [sodium(2-sulfonatoethyl) methanethiosulfonate], MTSET (2-(trimethylammonium)ethyl methanethiosulfonate bromide), and MMTS (methyl methanethiosulfonate) were purchased from Toronto Research Biochemicals (Downsview, ON, Canada), maleimide reagents were from Molecular Probes, and all other reagents were from Sigma or Research Organics, except as noted.

Fluorescence and Electrophysiological Experiments. Oocytes were labeled with 100 μM tetramethylrhodamine-6-maleimide (TMR6M) while voltage clamped (−100 mV) in NaCl buffer (in mM: 100 NaCl/2 KCl/1 $MgCl_2$/10 Hepes, pH 7.5) for 4 min at 20°C, then transferred into a NaCl buffer solution free of the dye, and maintained in the dark until use. The experiments were performed by using the two-electrode voltage clamp on the stage of an inverted epi-fluorescence microscope (15). For measurements of fluorescence, the oocyte membrane was illuminated with a 150-W tungsten lamp and excitation and emission filters at 535 and 605 nm (XF33, Omega Optical, Brattleboro, VT). Fluorescence was measured with a Hamamatsu HC125–01 photomultiplier tube (Bridgewater, NJ) connected to the camera port of the microscope. An electronic shutter was placed between the lamp and the preparation to minimize photobleaching. The fluorescence signal and the presteady–state currents were digitized at 400 μs per point and low-passed at 500 Hz with an 8-pole Bessel filter (Frequency Devices, Havenhill, MA). Electrophysiological and fluorescence experiments were performed simultaneously by using a pulse protocol in which the membrane voltage was stepped for 100 ms from the holding potential (typically −100 mV) to a series of test voltages, starting at +50 mV and ending at −150 mV in 20-mV steps (6). At each voltage, the presteady–state currents and the fluorescence traces were measured from an average of three runs. Fluorescence changes (ΔF) were quantified as the % change from baseline (ΔF/F). All experiments were performed under continuous superfusion of the bath solution. Steady–state sugar-induced currents I (difference in current before and after addition of sugar) were fitted to the equation $I = I_{max}[S]^n/([S]^n + (K_{0.5})^n)$; [S] is the substrate ($Na^+$ or αMDG) concentration, I_{max} is the maximal current at saturating [S], $K_{0.5}$ is the substrate concentration at 0.5 I_{max}, and n is the Hill coefficient (16). All of the experiments were repeated on at least three oocytes from different donor frogs.

RESULTS

Changing the GGM Q457R mutation to Q457C restored full function to the SGLT1 protein. Fig. 1*A* shows the increase in current (180 nA) recorded at the holding potential (−50 mV) when 200 mM αMDG (α-methyl-D-glucopyranoside) was added to the NaCl buffer superfusing the oocyte. The αMDG-induced current was saturable with an affinity constant $K_{0.5}$ for αMDG of 6 mM (at −150 mV) and Na^+-dependent with a $K_{0.5}$ for Na^+ of 2.5 mM (at −150 mV). Similar experiments with wild-type human SGLT1 gave $K_{0.5}$ values of 0.35 mM for αMDG and 2.5 mM for Na^+ (see also ref. 16). The voltage dependence of these parameters was similar in mutant and wild-type cotransporters, i.e., the $K_{0.5}$ values for αMDG and Na^+ decreased in a similar fashion to minimum values as the membrane potential increased from −30 to −150 mV. These results, along with the presteady–state-kinetic measurements presented below, indicate that the Cys mutant is expressed in a fully functional form with a decrease in sugar affinity.

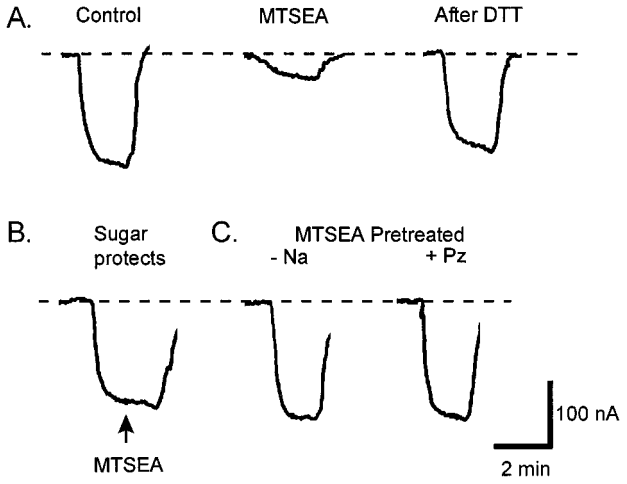

FIG. 1. Effects of substrates on MTSEA labeling of Q457C. The ability of 1 μM MTSEA to label the Q457C residue was influenced by substrate binding. A single Q457C-expressing oocyte was voltage-clamped at −50 mV in Na buffer as the composition of the bath solution was varied. Effects on Q457C function were measured as current generated by 200 mM αMDG. (*A*) Control. αMDG generated a current of 180 nA. After reequilibration in Na buffer, the oocyte was exposed to MTSEA for 80 sec. This resulted in inactivation of transport; the current was reduced to 40 nA. Complete recovery from MTSEA inactivation was achieved by washing the oocyte in 10 mM DTT in Na buffer for 15 min. (*B*) Sugar was able to prevent MTSEA inactivation. After addition of 200 mM αMDG, 1 μM MTSEA (arrow) was added to the bath for 80 sec; no reduction in current was observed. (*C*) There was no reduction in αMDG-induced current if the oocyte was pretreated with MTSEA in the absence of Na^+ (choline replacement) or in the presence of Na^+ and 100 μM phlorizin before testing for αMDG transport. Between all of the experiments, the oocyte was washed in 10 mM DTT for 15 min before equilibration in Na buffer. Dashed line indicates baseline holding current.

Chemical mutagenesis of Q457C by alkylating reagents abolished sugar transport. Pretreatment with 1 μM MTSEA for 80 sec reduced the αMDG-dependent current by 80% (Fig. 1*A*). This inhibition was reversed by treating the oocyte with 10 mM DTT for 15 min. Increasing either the MTSEA concentration or the time of exposure resulted in complete inhibition. MTSEA caused an increase in the Na^+-leak current, i.e., the Na^+-uniport mode of Na^+ transport in the absence of sugar (16). The leak currents were measured before and after complete reaction of Q457C with MTSEA by measuring the phlorizin-sensitive currents in the absence of sugar: in a pair of experiments, the currents at −150 mV were 150 and 112 nA before and 337 and 290 nA after MTSEA. In control experiments, the wild-type SGLT1 was completely insensitive to MTSEA, other MTS reagents, and NEM, e.g., exposing SGLT1-expressing oocytes to 1 mM MTSEA for up to 10 min had no effect on αMDG-induced currents (not shown). This indicates that: (*i*) the native cysteines in SGLT1 are either inaccessible to −SH reagents or that alkylating these residues has no functional effect, and (*ii*) MTSEA reacts with cysteine 457 in the mutant protein to inhibit sugar transport. Similar results were obtained with ^{14}C-αMDG-uptake measurements on oocytes expressing Q457C and wild-type SGLT1 proteins (M. Panayotova-Heiermann, unpublished observations). Other sulfhydryl reagents, MTS and NEM derivatives, inhibited sugar transport by Q457C in 22 other experiments but with varying potencies. The potencies were obtained by determining the concentration of the reagent required to produce 50% inhibition after 2-min exposure: the relative potencies were $MTSEA^+(500) > MTSET^+(5)$, MMTS(5) > $MTSES^-(1)$, NEM(1), and TMR6M(1). As anticipated, the effect of NEM derivatives was not reversed by DTT.

MTSEA and NEM react with the same cysteine residue in Q457C SGLT1 because: (*i*) the fraction of transport remaining after incomplete reaction with one reagent could be obliterated by addition of the other; (*ii*) there was no additive effect of NEM after complete inhibition of transport with MTSEA; (*iii*) the effect of MTSEA, but not NEM, was completely reversible with DTT; and (*iv*) 50% inhibition by MTSEA, followed by complete inhibition by NEM was only 50% restored after DTT.

Alkylation of Q457C depended on the presence or absence of ligands. No MTSEA inhibition was observed if the reaction occurred in the presence of 200 mM αMDG (Fig. 1*B*), and no inhibition was obtained when oocytes were pretreated with MTSEA either in the absence of Na^+ (Fig. 1*C*) or in the presence of 100 mM Na^+ and 100 μM phlorizin. Finally, we observed that the inhibition produced by MTSEA treatment in 100 mM Na^+ depended on the membrane potential of the oocyte (Fig. 2). MTSEA inhibited the αMDG-induced current only 20% when the membrane potential was clamped at 0 mV during the reaction, whereas inhibition was 80% at −100 mV. Intermediate effects were obtained between 0 and −100 mV. The voltage dependence of accessibility was the same with all of the other MTS and NEM derivatives tested, including positively charged ($MTSEA^+$), neutral (MMTS), and negatively charged ($MTSES^-$) reagents (not shown). This result suggests that: (*i*) the effect of voltage is on the protein itself rather than on the reagent, and (*ii*) residue 457 is not in the membrane electric field, otherwise membrane potential would electrophoretically exert differential effects on the apparent reactivities, reflecting the valence of the reagent.

Membrane potential has been shown to affect transporter function, i.e., the presteady–state currents indicate that partial reactions of the transport cycle are voltage dependent (6, 17). We suspected that there may be a relationship between presteady–state currents and the rate of alkylation of Cys457. Therefore, we compared the presteady–state Q457C SGLT1 currents in response in voltage-jumps (see Fig. 4*A*) and the effect of voltage on MTSEA inhibition of αMDG-induced currents in a single oocyte. Integration of the presteady–state currents at each test potential gives the Q457C charge movement Q, and the Q measured at each voltage is plotted in Fig. 2. The charge/voltage (Q/V) curve was fitted to a Boltzmann function to obtain: (*i*) Q_{max}, the maximum charge movement; (*ii*) $V_{0.5}$, the voltage giving 0.5 Q_{max}; and (*iii*) **z**, the apparent valance of the moveable charge. For Q457C SGLT1, the maximum charge transfer varied between 8–14 nC, depending on expression level, $V_{0.5}$ was −25 to −35 mV, and **z** was ≈1; values similar to those obtained for the human wild-type SGLT1 protein (6). It is apparent from Fig. 2 that there is a close correlation between membrane potential and accessibility to labeling and charge movement.

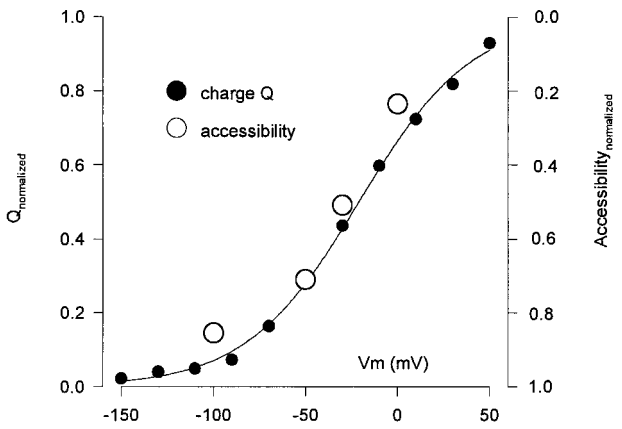

FIG. 2. Correlation of the voltage dependence of Q457C accessibility and the presteady–state charge movement. Accessibility was measured as the extent of inhibition of the sugar-induced current (unity is 100%) after 1 min exposure to 10 μM MTSEA. The relative voltage sensitivity was obtained by normalizing the accessibility at the usual holding potential (−50 mV) to the charge. At each test voltage, the charge Q was obtained by integration of the presteady–state currents (see Fig. 4*A*). The curve was the fit of the Q/V data to the Boltzmann relation (6): $(Q - Q_{hyp})/Q_{max} = 1/[1 + \exp(z(V - V_{0.5})F/RT)]$. $Q_{max} = Q_{dep} - Q_{hyp}$; Q_{dep} and Q_{hyp} are Q at depolarizing and hyperpolarizing limits, z is apparent valence of the movable charge, $V_{0.5}$ is voltage at 0.5 Q_{max}, F is Faraday, R is the gas constant, and T is absolute temperature. In this experiment, $Q_{max} = 13 \pm 1$ nC, $z = 0.8 \pm 0.1$, and $V_{0.5} = -21 \pm 3$ mV (statistics are errors of the fit). The data has been normalized between 0 and 1.

After complete reaction of Q457C with MTSEA, αMDG binds to the protein even in the absence of sugar transport. Although there was no measurable change in the Q/V parameters in the absence of sugar (not shown), when sugar was added, the Q/V curve shifted along the voltage axis (Fig. 3*A*). This shift in $V_{0.5}$ with sugar was not accompanied by changes in either Q_{max} or **z**. The αMDG-induced shift in $V_{0.5}$, $\Delta V_{0.5}$, was a saturable function of the sugar concentration with a $K_{0.5}$ of 12 mM (Fig. 3*B*).

These results suggest that the accessibility of Q457C to alkylating reagents depends on the conformational state of the cotransporter. To examine this more directly, we labeled the protein with a fluorescent NEM derivative, TMR6M, and measured fluorescence as a function of voltage. TMR6M blocked αMDG transport irreversibly, and, as with the MTS reagents (Figs. 1 and 2), the degree of inhibition was Na^+- and voltage-dependent and labeling was blocked by sugar and phlorizin (not shown). The 5-isomer tetramethylrhodamine-5-maleimide (TMR5M) did not label the protein (and therefore did not block sugar transport) under the same labeling conditions. Q457C was labeled completely with 0.1 mM TMR6M in 100 mM Na^+ buffer at −100 mV, and we simultaneously recorded both charge movements and fluorescence in response to voltage-jumps. When the membrane potential was stepped from V_h of −100 mV to test potentials up to

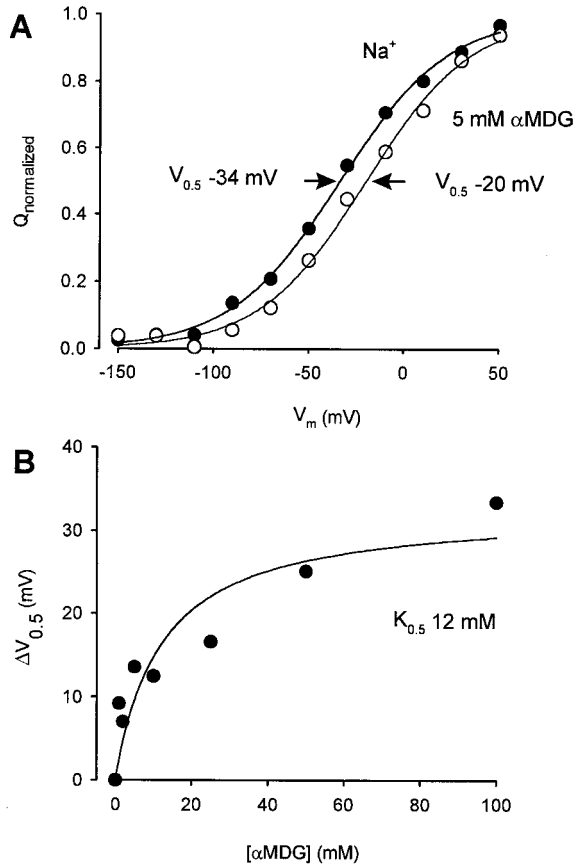

FIG. 3. Sugar binding to Q457C. The binding of sugar to Q457C can be studied from the effect of external sugar on the presteady–state charge movement. Sugar shifted the $V_{0.5}$ of the Q/V relation. (*A*) The effect of sugar on Q/V relations. Normalized Q/V curves at 0 and 5 mM αMDG. The $V_{0.5}$ of the Q/V curve at 5 mM αMDG shifted +14 mV. Fits to the data gave, in Na^+: Q_{max} 13 ± 1 nC, z = 0.9 ± 0.1, $V_{0.5}$ = −34 ± 2 mV; in 5 mM αMDG: Q_{max} = 12 ± 1 nC, z = 0.9 ± 1, and $V_{0.5}$ = −20 ± 4 mV. (*B*) Dependence of the $V_{0.5}$ on external sugar concentration. The curve was drawn according to the equation: $\Delta V_{0.5} = \Delta V_{max}[\alpha MDG]/(K_{0.5} + [\alpha MDG])$ with ΔV_{max} = 33 ±5 mV and $K_{0.5}$ = 12 ± 6 mM.

+50-mV transient currents were observed, and transient currents in the opposite direction were seen when the membrane potential was returned to the holding voltage (Fig. 4*A*). At each test voltage the charge transfer (Q), the integral of the transient currents, was equal for the ON and OFF responses. Q as a function of the test voltage is plotted in Fig. 4*D*, and the time constants for the current relaxations (τ) are plotted against the test voltage in Fig. 4*E*. Rhodamine labeling had no effect on the presteady–state charge movement as both the Q/V and τ/V curves were identical before and after complete labeling of Q457C with TMR6M (not shown).

The rhodamine fluorescence recorded during the voltage-jumps is shown in Fig. 4*B*. There was a reversible quench in fluorescence that became larger with larger membrane depolarizations: at each voltage, the steady–state change in fluorescence (ΔF) was directly proportional to the charge moved Q (Fig. 4*D*), and the time constant for the fluorescent quench was proportional to the time constant for the current relaxation (Fig. 4*E*). The time constants for the recovery of the fluorescence at the end of the voltage pulse were faster than those for the current relaxations. In this experiment, the membrane potential was held at −100 mV. Hyperpolarizing voltage steps resulted in a small charge movement, which was accompanied by a small increase in fluorescence, e.g., −150 mV (Fig. 4*A* and *B*). When membrane potential was held at a value (e.g., −50 mV) close to the $V_{0.5}$ (−30 mV), the charge movement and the fluorescence changes were symmetric in the depolarizing and hyperpolarizing directions (not shown). Finally, both the charge movements and the fluorescence changes were blocked by 100 μM phlorizin (Fig. 4*C*). These experiments demonstrate that the Q457C charge movements are closely accompanied by changes in rhodamine fluorescence.

DISCUSSION

Key findings of this study are that conformational changes are responsible for the coupling of sugar and Na^+ transport and that presteady–state charge distribution reflects conformational states of the protein. Voltage and substrates affect the presteady–state charge distribution and also, as shown here, the ability of the reagents to label Q457C.

The discovery of the mutation Q457R in a GGM patient identified Q457 as a critical residue (11). We have found that this defect in sugar absorption is caused by a blockade in sugar transport without causing any reduction in uncoupled Na^+ transport ("leak") or large changes in the kinetics of presteady–state charge movement. In contrast, the present study shows that replacing Arg with Cys (Q457C) fully restores Na^+/glucose cotransport. The $K_{0.5}$ for Na^+/αMDG cotransport, the Na^+-leak, and the characteristics of voltage-dependent charge movement (Q/V and τ/V curves) were all similar to the wild-type protein. Chemical mutagenesis of Q457C with a wide range of MTS and NEM derivatives recapitulated the properties of the Q457R; i.e., sugar translocation was blocked completely (Fig. 1*A*) even though sugar binding (apparent K_d 12 mM, Fig. 3), the Na^+-leak, and the charge/voltage relationship (Fig. 4) were relatively unchanged. This result indicates that the defect with the GGM mutant is primarily caused by the increased bulk of the side chain at residue 457, i.e., with Arg or with modification of Cys with $MTSEA^+$, $MTSET^+$, MMTS, $MTSES^-$, NEM, and TMR6M and that the effect is confined to preventing sugar translocation.

We have proposed a six-state ordered kinetic model for Na^+/glucose cotransport (4, 6, 17, 18). The model describes Na^+/glucose cotransport as a series of ligand-induced conformational changes (Fig. 5). On the external surface of the membrane, two Na^+ ions bind to the transporter before sugar. The empty transporter C (states 1 and 6), the Na^+-loaded transporter CNa_2 (states 2 and 5), and the sugar-loaded transporter CNa_2S (states 3 and 4) can "cross" the membrane. Membrane voltage affects Na^+ binding and translocation of the empty transporter across the membrane. Our present data provides further support for this model. Although alkylating reagents completely blocked Na^+/sugar transport by Q457C SGLT1, the rate of alkylation critically depended on the presence and absence of ligands and membrane voltage. Maximum accessibility occurred in the presence of external Na^+ when membrane voltage was held at −100 mV (Fig. 2), and access was blocked by reducing the voltage toward 0 mV, adding sugar, phlorizin (the potent inhibitor of Na^+/glucose cotransport), or replacing external Na^+ with choline (Fig. 1). Thus, Q457C is only accessible to the reagents in the CNa_2 conformation. Our data provide evidence that SGLT1 exists in at least three conformations (C, CNa_2, CNa_2S, and/or the phlorizin-bound state CNa_2Pz). The relationship between the fraction of the total protein in the CNa_2 conformation, voltage and the concentration of substrates is predicted by computer simulations of our six-state model (4).

Further direct evidence that transitions between these conformational states are relevant to the mechanism of Na^+/glucose cotransport comes from voltage-jump experiments on Q457C SGLT1 labeled with TMR6M (Fig. 4). The simultaneous recording of SGLT1 currents and rhodamine fluores-

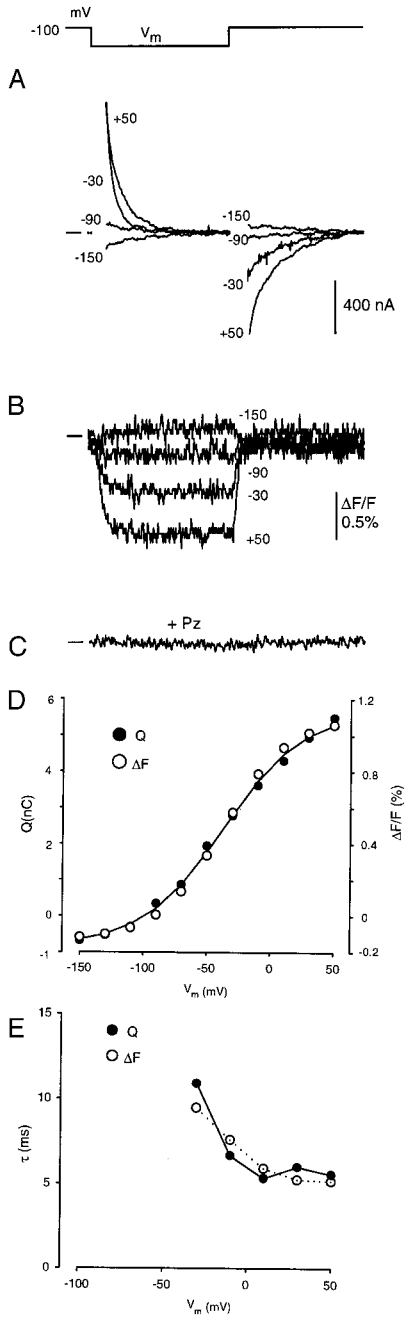

FIG. 4. Relationship between presteady–state charge movement of Q457C labeled with TMR6M and the quench in fluorescence. (*A*) Presteady–state current records. Membrane potential was stepped for 100 ms from the holding potential (−100 mV) to a series of test values from +50 to −150 mV in 20 mV decrements. The total current I was fitted to the equation: $I(t) = I_1\exp(-t/\tau_1) + I_2\exp(-t/\tau_2) + I_{ss}$; where t is time, $I_1\exp(-t/\tau_1)$ is the capacitive transient with initial value I_1 and time constant τ_1, $I_2\exp(-t/\tau_2)$ is the presteady–state current of Q457C with initial value I_2 and time constant τ_2, and I_{ss} is the steady–state current. Q457C presteady–state current was obtained from the total current by subtraction of the capacitive and steady–state currents (6). The solid line at the left is baseline. (*B*) Time course of the voltage-sensitive quench of rhodamine fluorescence. Fluorescence was monitored simultaneously in the experiment of Fig. 4*A*. (*C*) Blockade of the voltage-dependent quench of rhodamine fluorescence by phlorizin. Addition of 1 mM phlorizin (Pz) to the external solution completely and reversibly abolished the voltage-dependent fluorescence quench. Phlorizin also inhibited the presteady–state currents (not shown). The time scale is the same for *A*, *B*, and *C*; the pulse duration is 100 ms. (*D*) Comparison of the Q/V and ΔF/V relations. The smooth curve was drawn according to the Boltzmann relation with $Q_{max} = 6.5$ nC, z = 1.0, and $V_{0.5} = -37$ mV. The voltage dependence of the quench of rhodamine fluorescence was identical to that of the presteady–state charge movement. (*E*) Correlation between the relaxation time constants τ of presteady–state current and the quench in rhodamine fluorescence.

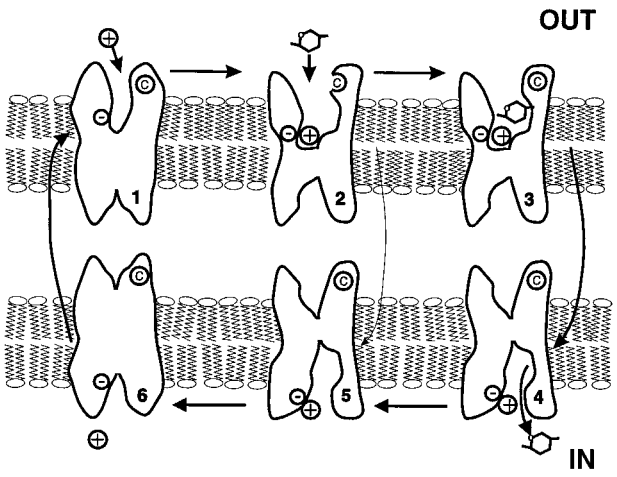

FIG. 5. Cartoon of the 6-state ordered kinetic model for Na^+/glucose cotransport. States 1–3 and 4–6 face the external and internal membrane surfaces, respectively. In the absence of ligands, the transporter exists in 2 states (1 and 6). At the external surface, 2 Na^+ ions bind to the transporter to form the complex CNa_2 (state 2). The fully loaded transporter CNa_2S (state 3) undergoes a conformational change (state 3 to 4) resulting in Na^+/glucose cotransport. The reaction from state 2 to 5 represents the uniport ("leak") pathway. Presteady–state currents are due to the partial reactions: $2 \rightleftharpoons 1 \rightleftharpoons 6$. Note that the cysteine © at residue 457 is only accessible in state 2, and that it most probably is not within the membrane electric field.

cence showed that voltage-dependent charge movements Q were accompanied by fluorescence changes (ΔF). Both the time course and the magnitude of the changes in fluorescence closely followed the kinetics of charge transfer. Phlorizin inhibited both Q and ΔF. These charge movements and fluorescence changes, along with the voltage-dependence of MTS and NEM labeling, and effects on Na^+/glucose cotransport (Fig. 2) clearly point to a fundamental role of conformational changes in the cotransport mechanism. The observed conformational changes with changes in accessibility strongly argues against the pore model for Na^+/glucose cotransport. Our data also is consistent with earlier fluorescence studies on rabbit SGLT1 in brush border membrane vesicles (19). Furthermore, the model predicts a rapid component of charge movement (17), and preliminary experiments with the cut-open oocyte preparation (20) indicate a close correlation between rapid components of charge movement and rhodamine fluorescence ($\tau \approx 100$ μs).

The quench of rhodamine fluorescence indicates an environmental shift of the reporter group. Although we do not yet have information about the nature of the quench, e.g., whether it is caused by a change in the Stokes-shift, our results suggest that Q457C is not within the membrane electric field and so environmental changes probably involve rearrangement of extramembrane domains. There must be substantial steric hindrance in the path to Q457C because the six-isomer (TMR6M) reacts with Q457C, whereas the five-isomer (TMR5M) does not interact. This suggests that the architecture of the vestibule to Q457C determines the selectivity between the two isomers. It also should be noted that the vestibule to the sugar-binding domain of SGLT1 also determines the selectivity for the transport of large bulky aromatic glucosides, β-phenyl and naphthyl glucosides are transported whereas α-phenyl and naphthyl glucosides are not (21). For

example, phlorizin, an aromatic β-glucoside, is a specific, high affinity, competitive blocker of Na^+/glucose cotransport (17).

In summary, we have shown that residue Q457 plays a critical role in sugar translocation through SGLT1 and that access to the cysteine mutant Q457C is correlated directly with the probability of the cotransporter being in the CNa_2 conformation (state 2, Fig. 5). In addition, by labeling Q457C with a fluorescent NEM derivative, we have demonstrated that voltage-dependent conformational changes are linked intimately to local environmental changes of Q457C. We conclude that cotransport of Na^+ and glucose occur as a consequence of conformational changes in the protein. We further suggest that sugar translocation is through the C-terminal domain (TMH 10–13) and that Na^+ binding to the N-terminal domain results in the conformational changes leading to Na^+, sugar, and water transport. In view of the common general properties of presteady–state and steady–state currents amongst cotransporters (1), our conclusions may be applicable to other cotransporters.

We thank Ms. M. Contreras and D. Leung for assistance with the oocytes; J. Parker for help with construction of the microscope; A. Cha and Dr. F. Bezanilla for valuable discussions on fluorescence experiments; S. Eskandari, Drs. I. Forster and M. Panayotova-Heiermann for comments on the manuscript. This work was supported by National Institutes of Health Grants DK19567, GM52094, and NS25554, and National Science Foundation Grant MCB 9520599.

1. Wright, E. M., Loo, D. D. F., Hirayama, B. A. & Turk, E. (1996) *Curr. Opin. Cell Biol.* **8,** 468–473.
2. Loo, D. D. F., Zeuthen, T., Chandy, G. & Wright, E. M. (1996) *Proc. Natl. Acad. Sci. USA* **93,** 13367–13370.
3. Schultz, S. G. & Curran, P. F. (1970) *Physiol. Rev.* **50,** 637–718.
4. Parent, L., Supplisson, S., Loo, D. D. F. & Wright, E. M. (1992) *J. Membr. Biol.* **125,** 63–79.
5. Su, A., Mager, S., Mayo, S. L. & Lester, H. A. (1996) *Biophys. J.* **70,** 762–777.
6. Loo, D. D. F., Hazama, A., Supplisson, S., Turk, E. & Wright, E. M. (1993) *Proc. Natl. Acad. Sci. USA* **90,** 5767–5771.
7. Akabas, M. H., Stauffer, D. A., Xu, M. & Karlin, A. (1992) *Science* **258,** 307–310.
8. Yang, N., George, A. L. & Horn, R. (1996) *Neuron* **16,** 113–122.
9. Chen, J.-G., Liu-Chen, S. & Rudnick, G. (1997) *Biochem.* **36,** 1479–1486.
10. Cheung, M. & Akabas, M. H. (1997) *J. Gen. Physiol.* **109,** 289–299.
11. Martín, G. M., Turk, E., Lostao, P., Kerner, C. & Wright, E. M. (1996) *Nat. Genet.* **12,** 216–220.
12. Turk, E., Kerner, C. J., Lostao, M. P. & Wright, E. M. (1997) *J. Biol. Chem.* **271,** 1925–1934.
13. Turk, E. & Wright, E. M. (1997) *J. Memb. Biol.* **159,** 1–20.
14. Panayotova-Heiermann, M., Eskandari, S., Turk, E., Zampighi, G. A. & Wright, E. M. (1997) *J. Biol. Chem.* **272,** 20324–20327.
15. Mannuzzu, L. M., Moronne, M. M. & Isacoff, E. Y. (1996) *Science* **271,** 213–216.
16. Hirayama, B. A., Lostao, M. P., Panayotova-Heiermann, M., Loo, D. D. F., Turk, E. & Wright, E. M. (1996) *Am. J. Physiol.* **270,** G919–G926.
17. Hazama, A., Loo, D. D. F. & Wright, E. M. (1997) *J. Membr. Biol.* **155,** 175–186.
18. Mackenzie, B., Loo, D. D. F. & Wright, E. M. (1998) *J. Membr. Biol.*, **162,** 101–106.
19. Peerce, B. E. & Wright, E. M. (1994) *Proc. Natl. Acad. Sci. USA* **81,** 2223–2226.
20. Cha, A. & Bezanilla, F. (1997) *Neuron* **19,** 1127–1140.
21. Lostao, M. P., Hirayama, B. A., Loo, D. D. F. & Wright, E. M. (1994) *J. Membr. Biol.* **142,** 161–170.